This paper describes objective technical results and analysis. Any subjective views or opinions that might be expressed in the paper do not necessarily represent the views of the U.S. Department of Energy or the United States Government.

SAND2021-15819J

Concentration-Dependent Ion Correlations Impact the Electrochemical Behavior of Calcium Battery Electrolytes

Nathan T. Hahn,[a,b,*] Julian Self,[a,c,d] Darren M. Driscoll,[a,e] Naveen Dandu,[a,f] Kee Sung Han,[a,g] Vijayakumar Murugesan,[a,g] Karl T. Mueller,[a,g] Larry A. Curtiss,[a,f] Mahalingam Balasubramanian,[a,e] Kristin A. Persson,[a,d,h] Kevin R. Zavadil[a,b]

[a]Joint Center for Energy Storage Research, Lemont, IL, 60439

[b]Material, Physical and Chemical Sciences Center, Sandia National Laboratories, Albuquerque, NM 87185

[c]Energy Technologies Division, Lawrence Berkeley National Laboratory, Berkeley, CA 60439

[d]Department of Materials Science and Engineering, UC Berkeley, CA 94720

[e]Advanced Photon Source, Argonne National Laboratory, Lemont, IL, 60439

[f]Materials Science Division, Argonne National Laboratory, Lemont, IL, 60439

[g]Physical and Computational Sciences Directorate, Pacific Northwest National Laboratory, Richland, WA 99354

[h]Molecular Foundry, Lawrence Berkeley National Laboratory, Berkeley, CA 94720

Abstract

Ion interactions strongly determine the solvation environments of multivalent electrolytes even at concentrations below that required for practical battery-based energy storage. This statement is particularly true of electrolytes utilizing ethereal solvents due to their low dielectric constants. These solvents are among the most commonly used for multivalent batteries based on reactive metals (Mg, Ca) due to their reductive stability. Recent developments in multivalent electrolyte design have produced a variety of new salts for Mg^{2+} and Ca^{2+} that test the limits of weak coordination strength and oxidative stability. Such electrolytes have great potential for enabling full-cell cycling of batteries based on these working ions. However, the ion interactions in these electrolytes exhibit significant and non-intuitive concentration relationships. In this work, we investigate a promising exemplar, calcium tetrakis(hexafluoroisopropoxy)borate ($Ca(BHFIP)_2$), in the ethereal solvents 1,2-dimethoxyethane (DME) and tetrahydrofuran (THF) across a concentration range of several orders of magnitude. Surprisingly, we find that effective salt dissociation is lower at relatively dilute concentrations (e.g. 0.01 M) than at higher concentrations (e.g. 0.2 M). Combined experimental and computational dielectric and X-ray spectroscopic analyses of the changes occurring in

Sandia National Laboratories is a multimission laboratory managed and operated by National Technology & Engineering Solutions of Sandia, LLC, a wholly owned subsidiary of Honeywell International Inc., for the U.S. Department of Energy's National Nuclear Security Administration under contract DE-NA0003525.

the Ca^{2+} solvation environment across these concentration regimes reveals a progressive transition from well-defined solvent-separated ion pairs to de-correlated free ions. This transition in ion correlation results in improvements in both conductivity and calcium cycling stability with increased salt concentration. Comparison with previous findings involving more strongly associating salts highlights the generality of this phenomenon, leading to important insight into controlling ion interactions in ether-based multivalent battery electrolytes.

Introduction

Multivalent batteries based on Ca^{2+}, Mg^{2+}, Zn^{2+}, or Al^{3+} are intriguing energy storage options due to the high energy densities of their corresponding metal anodes. Ca in particular has received growing interest due to its negative metal redox potential, approaching even that of Li, and its polarizability,[1-2] which may facilitate cationic transport through intercalation host materials.[3] However, its significant negative redox potential (-2.87 V vs. SHE) greatly limits the scope of stable electrolytes that can support reversible Ca metal electrochemistry. Much like the early years of Mg electrolyte development,[4-5] initial room temperature Ca electrolyte demonstrations have originated from an electrolyte containing a reducing salt ($Ca(BH_4)_2$) dissolved in the ethereal solvent tetrahydrofuran (THF).[6] However, such reducing salt species are easily oxidized, precluding the operation of high voltage cells. Among the most intriguing oxidatively stable alkaline earth metal salts to be developed in recent years are fluorinated alkoxy-borates and aluminates.[7-11] A particularly significant borate example is based on the tetra-substituted hexafluoro-isopropoxy ligand, $BHFIP^-$. Both the Mg and Ca salts of this anion can be used to reversibly electrodeposit the corresponding metal in ether solvents, and they exhibit high oxidative stability limits.[8-9, 11] Furthermore, these salts are soluble in most relevant electrolyte solvents and dissociate very easily due to the extreme charge-delocalization of the bulky $BHFIP^-$ anion,[12-13] leading to high ionic conductivities and metal deposition/stripping rates. Therefore, $BHFIP^-$ salts represent an extreme case of super-weak anion-cation coordination and allow us to understand the practical limits of ethereal solvent based electrolytes. Understanding how the solvation environment of these salts influences their electrochemical behavior is

thus important from the standpoint of state-of-the-art multivalent battery development and of electrolyte science in ethereal solvents, which is critical for beyond Li-ion battery technologies in general.

While ethereal solvents are advantageous in battery electrolytes supporting metal anodes due to their high reductive stability, they possess small dielectric constants ($\varepsilon_r \sim 7$) and tend to produce lower ionic conductivities than most polar aprotic solvents, particularly in multivalent systems.[14] Indeed, significant ion pair formation and aggregation is a common observation in Mg^{2+} and Ca^{2+} electrolytes and can throttle ionic conductivity to prohibitive extents, as observed in borohydride electrolytes.[1, 15-16] Even in the case of super-weakly coordinating anions such as $BHFIP^-$, there is a need to understand the interplay between solvation structure and ion correlations that may arise due to strong interionic forces, even if contact ion pairs (CIPs) are not prevalent.[13] Furthermore, the dependence of these features on salt concentration can be non-intuitive, and the degree to which they can be harnessed to control electrolyte function is an important insight informing electrolyte design and development. For example, the effectiveness of ionic species formation (i.e. ionicity) has been found to improve with an increase in salt concentration for both the strongly associating $Ca(BH_4)_2$ in THF as well as the more weakly associating $Mg(TFSI)_2$ in 1,2-dimethoxyethane (DME) or diglyme, despite significant differences in their relative association tendencies.[1, 16-17] These observations point to a general trend in solvation behavior across disparate association regimes that might be extended to even the most weakly associating salts.

Toward this end we report an investigation of the concentration-dependent ion correlations of $Ca(BHFIP)_2$ solutions in the simple ethereal solvents DME and THF. We confirm that the generalized positive relationship between effective salt ionicity and concentration does indeed apply to these electrolytes. We further demonstrate through spectroscopic and computational interrogation that these effects originate from significant changes in ion pair populations. In particular, combining the dipolar cluster speciation from dielectric relaxation spectroscopy and molecular dynamics (DRS-MD) with the Ca-specific solvation environment from X-ray absorption spectroscopy and time-dependent Density Functional Theory (XAS-TD-DFT) provides important, atomistic insight into the 2nd solvation shell structure of Ca^{2+}.

These techniques enable identification of the primary ion pair species in these electrolytes as the solvent-separated ion pair (SSIP), which is a species not easily identified by other techniques. Finally, we evaluate the impact of these measured changes in Ca^{2+} solvation environment on calcium cycling behavior.

Methods

Electrolyte Preparation: Electrolyte synthesis was performed inside a catalyst-purified, argon filled glove box (MBraun) with typical water and oxygen levels below 1 ppm and 0.1 ppm, respectively. All reagents were purchased from Sigma-Aldrich. DME and THF were distilled over sodium and stored over activated alumina and 3A molecular sieves prior to use, yielding measured water levels < 5 ppm. These ethereal solvents are volatile, flammable, and have the potential for peroxide formation, necessitating appropriate measures for handling and storage. $Ca(BHFIP)_2$ salts were synthesized from $Ca(BH_4)_2$ and molecular sieve-dried hexafluoroisopropanol (99.9%) as solvates in either DME or THF, depending on the electrolyte solvent to be characterized, consistent with previously reported methodology.[12] Solution makeup involved using total volume rather than solvent volume as the basis for the reported molar concentrations. Electrochemical experiments were performed using recrystallized solvate material with purity greater than 99.5% based on ^{19}F nuclear magnetic resonance (NMR) and ~100% purity based on ^{11}B NMR. We were unable to achieve the requisite ^{19}F purity in THF solvates and thus electrochemical results are only reported for DME.

Electrochemical Characterization: Measurements were performed using a Solatron Modulab potentiostat. Ionic conductivity values were measured by electrochemical impedance spectroscopy using a calibrated custom cell with a cell constant verified through aqueous KCl measurements. Voltammetric measurements were performed in a small beaker-style three-electrode cell consisting of calcium rod reference and counter electrodes and a polished Au disc working electrode with 0.02 cm^2 exposed area (BASi). Correction for *IR* was performed by first measuring the uncompensated resistance between the working and reference by electrochemical impedance spectroscopy and then inputting this value into the voltammetry parameters within the potentiostat software. As noted in the text, several different potential scanning windows were

employed in order to optimize the calcium cycling response at each concentration. This was intended to account for variation in nucleation overpotential and deposition current density across the concentration range.

Pulsed Field Gradient Nuclear Magnetic Resonance: Diffusion coefficients, *D*, of $BHFIP^-$ anions and solvent molecules were measured at 25 °C by ^{19}F and ^{1}H PFG-NMR, respectively, on a 600 MHz NMR spectrometer (Agilent) equipped with 5 mm z-gradient probe (Doty Scientific) by employing a bipolar gradient stimulated echo sequence (Dbppste, VNMRJ). The ^{19}F and ^{1}H echo heights were observed with the increase of gradient strength (g) over 16 equal steps with fixed values of gradient duration (δ) of 2 ms and gradient distance (Δ) of 30 ms for all samples. Data were fitted with the Stejskal-Tanner equation,

$$S(g)=S(0)exp[-D(\gamma g\delta)^2(\Delta-\delta/3)] \quad (1)$$

where $S(g)$ and $S(0)$ are the echo heights at the gradient strength of g and 0, respectively. γ is the gyromagnetic ratio of ^{19}F ($2\pi\cdot40.078$ rad·MHz·T^{-1}) or ^{1}H ($2\pi\cdot42.577$ rad·MHz·T^{-1}).

Dielectric Relaxation Spectroscopy: DRS was performed in glass vials using a dielectric probe kit (Keysight N1501A) and vector network analyzer (Keysight 9375A) over a frequency range of 0.5 to 26.5 GHz. Each set of measurements were performed with three-point calibration using air, water, and THF. Duplicate measurements were performed after recalibration to verify consistency. Simultaneous fitting of the real and imaginary components of the complex permittivity was performed using one Debye relaxation for the solvent and one Cole-Cole relaxation for the ion pairs.[18] The Cole-Cole relaxation accounts for broadening ($\alpha > 0$) due to a distribution of relaxation time constants arising from ion pair configurational variability. This is physically reasonable given the size and flexibility of the $BHIP^-$ anion. The value of α was allowed to vary between 0 and 0.3 in these cases. The solvent relaxation frequencies were constrained to not exceed that measured for the neat solvent, which would be physically unreasonable. The solution ionic conductivity was treated as an adjustable fitting parameter but was constrained to differ from the independently measured conductivity by no more than 10 %. Due to the high ionic conductivity of the

concentrated samples, the lower frequency limit used for fitting ε" was increased from the instrumental limit of 0.5 GHz up to 0.6-1.0 GHz, depending on sample conductivity. This is generally necessary in DRS analyses to eliminate unphysical ε" responses that occur in such solutions.[19-20] The full range of ε' values (which are not affected by conductivity) were still maintained in every case.

X-ray Absorption Spectroscopy: XAS was performed at the Ca K-edge using beamline 9-BM and 20-BM of the Advanced Photon Source. Liquid electrolytes were dispersed onto porous polyolefin discs (Celgard, 25 μm in thickness) and sealed within an aluminized-mylar pouch. A Si(111) monochromator and a Rh coated mirror for harmonic suppression with a cutoff energy of 6 keV were both used. Measurements of the highly concentrated electrolytes (0.4-0.45 M) were acquired in transmission mode by dispensing each solution-phase electrolyte into a stack of Celgard to optimize the absorbance pathlength. Measurements of the dilute electrolytes were performed in fluorescence mode by positioning the sample at a 45° angle relative to the incident beam. Based on the concentration regime used within the experiments, self-absorption effects were expected to be minimal. The data were dead-time corrected to account for saturation effects of the fluorescence detector, and the total count rate did not exceed 80000 counts per second for each element at the Ca white line. The energy scale of the XAS data was calibrated by defining the first derivative maximum of a titanium foil absorption spectra as 4966 eV. Energy reproducibility was checked by periodically measuring the spectra of the Ti foil. XAS data were normalized to unit step height using the Athena software package.[21] X-ray absorption pre-edge structure was analyzed using XASViewer within Larch.[22] Pre-edge features were edge-subtracted using the combination of a Lorentzian to define the absorption edge and a linear function for the pre-edge background

Simulations and Computational Methods: Classical molecular dynamics (MD) simulations were used for the dielectric increment calculations, as discussed in previous publications.[17, 23] The herein used methodology is species-constrained MD, which differs from conventional MD simulations which have non-constrained speciation and more than one salt species in the simulation box (i.e. where equilibria is present between various free and associated salt species in solution). By using one salt species (free cation,

anion, CIP, SSIP etc.) in the simulation box, we can study the given ionic species' dielectric contribution while being assured of its identity. These salt species were placed in a box with 96 DME solvent molecules or 112 THF solvent molecules (approx. 0.10 M) using PACKMOL.[24] The SSIP species were simulated with constraints found via electronic structure methods (see below). Specifically, distances of 5.8 A for Ca-B_{BHFIP} in THF and 7.0 A for Ca-B_{BHFIP} in DME were used. No constraints were necessary for the free, CIP or neutral species. MD calculations were carried out with the GROMACS software.[25] The electrolyte systems studied were equilibrated first using a Berendsen barostat (NPT),[26] followed by heating and cooling steps. Afterwards, NVT ensemble production runs were undertaken using the velocity rescaling thermostat.[27] In the systems studied, the single salt species were associated for the duration of the simulation (each at least 10 ns). The dielectric constant of the entire electrolyte was found through consideration of the dipole moment of both solvent molecules and the associated salt species. The neat solvent dielectric constant was subtracted from the calculated dielectric constant of the studied electrolyte system, and this difference divided by the concentration (e.g. 0.10 M) provides the dielectric increment per salt species, as appearing in Table 1. In the case of associated salt species which have an overall charge (e.g. the SSIP or CIP), the charge multiplied by the center of mass distance was subtracted from the dipole moment as discussed in a previous publication.[17] The THF force field parameters were taken from Caleman et al.[28] and the Ca^{2+} forcefield parameters from the standard OPLS forcefield.[29-30] The $BHFIP^-$ anion and DME solvent molecule forcefield parameters were standards from OPLS, and the atomic charges were generated with Maestro software.[31] For the DME solvent molecule, the atomic charges were scaled by 0.82 to reproduce the neat solvent dielectric constant. We note that dielectric increment values calculated in MD are likely dependent on the forcefield parameters used, which could lead to dielectric increment changes if partial solvent or ionic charges are scaled by ~0.8x. Nevertheless, we found that such changes are small enough to not significantly affect the inferred speciation behavior or jeopardize the essential conclusions of the study (see supporting information, Figure S1). Error estimates for the dielectric increment values were calculated from duplicate simulations and analyses.

Electronic structure methods, which were used to generate Ca-B_{BHFIP} distance constraints in the SSIP structures, were undertaken with Gaussian software.[32] The ωB97X-D functional[33] was used with the 6-31+G(d,p) Pople basis set. Explicit solvent molecules were used (coordination numbers of 6 and 8 for THF and DME respectively), enhanced with a polarizable continuum model (ε_r = 7) to account for long-range electrostatic solvation effects.[34-35]

Time-dependent Density Functional Theory: Geometric relaxations of $[Ca(THF)_6]^{2+}$, $[Ca(DME)_4]^{2+}$ and $[Ca(THF)_6(BHFIP)_2]$ were performed using the TPSS functional and the def2tzvp basis set,[36] as implemented in the ORCA 4.2 code.[37] We then used TD-DFT to obtain the XAS spectra using the BHLYP functional and the def2tzvp basis set,[38-39] as this combination has proven to be most accurate in reproducing the pre-edge peaks by only slightly adjusting the energy of overall spectra.[13]

Results and Discussion

Significant non-monotonic changes in effective electrolyte ionicity occur across a wide range of $Ca(BHFIP)_2$ concentrations in both DME and THF. These changes are clearly demonstrated in the electrolyte molar conductivity (Λ), which represents the ionic conductivity divided by the molarity of the salt (Figure 1). In both solvents, Λ reaches a minimum at 0.005-0.01 M (Figure 1a). Λ then increases by approximately a factor of two as concentration is increased to 0.1 M. As concentration approaches the solubility limit (0.4-0.45 M), Λ begins to decrease again due to increasing viscosity and decreasing ion mobility. At concentrations below the range highlighted in Figure 1, Λ exhibits a monotonic decrease with increasing concentration, consistent with classical dilute electrolyte behavior (supporting information, Figure S2). It is noteworthy that nearly identical behavior is observed whether DME or THF is used as the solvent, despite their differences in structure, coordination strength, and coordination number toward Ca^{2+}.[12-13] The fact that the Λ vs. concentration trends are independent of these factors suggests that long-range interactions are responsible rather than differences in 1st solvation shell features. PFG-NMR measurements of $BHFIP^-$ diffusivity aid in interpreting these findings as the anion mobilities measured at 0.01, 0.1, and 0.4-0.45 M show a consistent decrease with increasing concentration, consistent with an

increase in viscosity (Figure 1b). The fact that Λ increases between 0.01-0.1 M despite a significant decrease in anion mobility indicates that de-correlation of cation-anion motion is occurring over this concentration range. The decrease in Λ observed at concentrations above 0.2 M indicates that de-correlation is no longer significant enough to overcome the reduced ion mobilities.

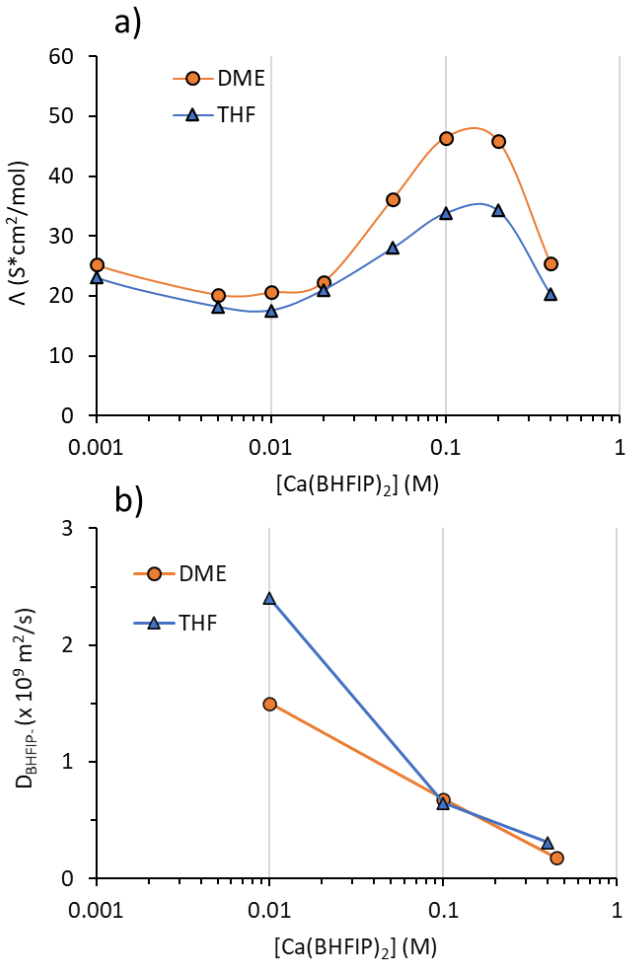

Figure 1. a) Molar conductivity values of $Ca(BHFIP)_2$ solutions in DME and THF solvents. b) Diffusion coefficients of the $BHFIP^-$ anions measured at select salt concentrations in these solvents by PFG-NMR. Additional conductivity and PFG-NMR data are contained in the supporting information document, Figure S2 and S3.

The observation of a Λ minimum at what would practically be considered very dilute salt concentrations is typical of electrolytes based on low permittivity solvents such as ethers or dialkyl carbonates.[1, 17, 40-42] Normally, such observations are reported for strongly associating salts such

borohydrides, but we find that this occurs even for an extremely weakly associating salt $Ca(BHFIP)_2$. This results from the persistence of interionic attraction over significant length scales, as quantified by the Bjerrum length, $\lambda_B = \frac{q_1 q_2}{4\pi\varepsilon_0 \varepsilon k_B T}$, where q_i represents the charges on the two ions of interest and ε_r is the solvent permittivity.[43] Indeed, even at 0.01 M the average interionic distance (38 Å) of a divalent 1:2 salt electrolyte calculated based on ion number density is much shorter than the corresponding λ_B of this electrolyte in DME (158 Å). By contrast, the corresponding λ_B of a 1:2 electrolyte in water (14 Å) is shorter than the interionic distance and thus Coulombic attraction is less than the thermal energy. In other words, even when "practically" dilute by electrochemical cell standards, ether-based electrolytes are not "theoretically" dilute in terms of their ionic interactions. Therefore, it is in fact reasonable to observe that the strong Coulombic interaction between Ca^{2+} and $BHFIP^-$ leads to significant correlated motion at low concentrations despite the extreme charge de-localization and weak coordination strength of the anion. An increase in Λ with increasing concentration, as we observe at 0.1-0.2 M has been historically attributed to various causes, including the conversion of neutral ion pairs to charged aggregates, such as triple ions in Li^+ electrolytes,[44] enhanced salt ionicity/dissociation due to the presence of significant CIP dipoles, i.e. CIP-induced "re-dissociation",[17, 45-46] or simply ion mobility enhancement independent of CIP formation.[47] In a recent investigation, we found that the average first solvation shell of Ca^{2+} in 0.2 M $Ca(BHFIP)_2$ solutions with either DME or THF as solvents contains little to no CIPs.[13] This result demonstrates that charged aggregates are not responsible for the elevated Λ values at these concentrations. Likewise, re-dissociation induced by a significant CIP population is also inconsistent with these results. Enhanced ionic diffusivities can also be ruled out based on the decreasing anion diffusivity reported herein. Although Ca^{2+} diffusivity is not measured, approximately one order of magnitude increase in D_{Ca} would be required to explain the Λ increase, which is unlikely. In other words, the usual explanations for an increasing Λ vs. concentration trend fall short in explaining the case of $Ca(BHFIP)_2$. Thus, a more thorough analysis of the solvation environment is needed to understand the origin of reduced ion correlations at elevated salt concentrations.

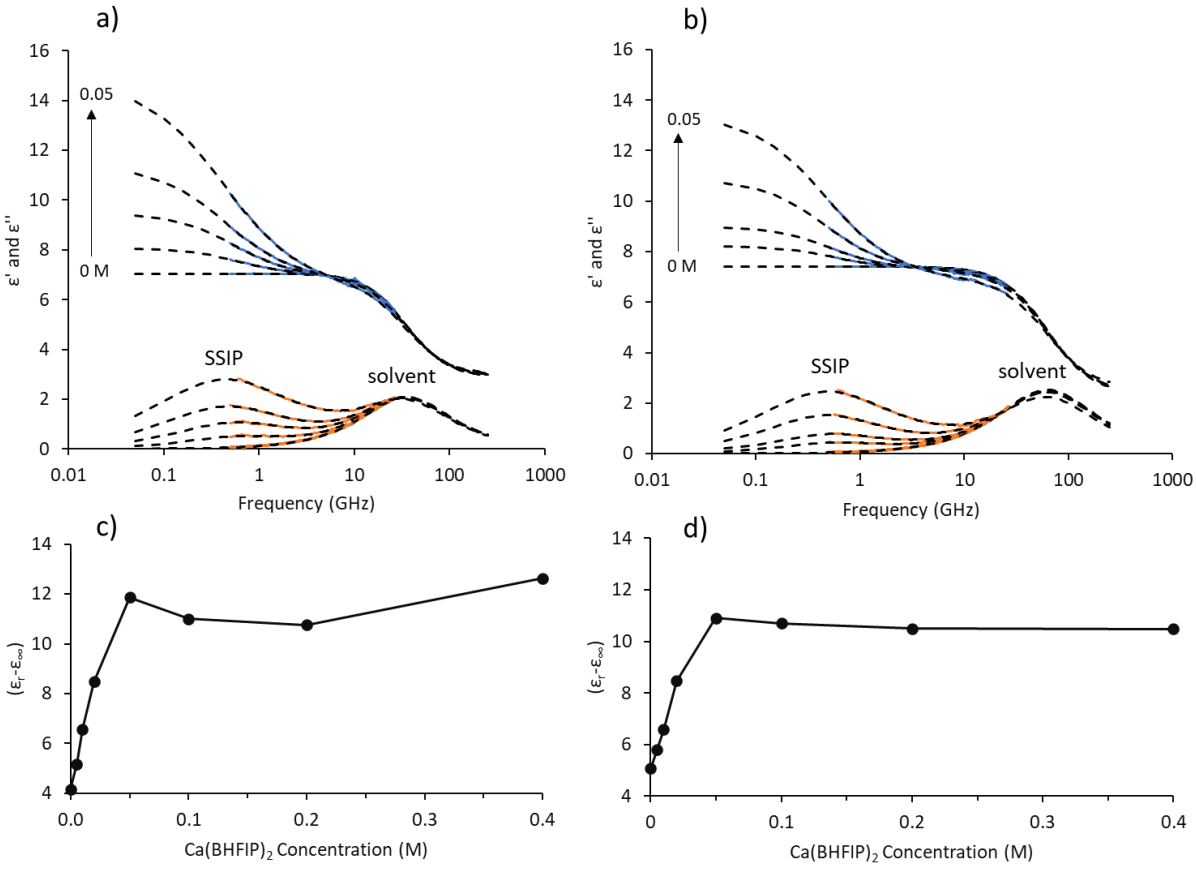

Figure 2. a,b) Complex permittivity spectra measured across the dilute $Ca(BHFIP)_2$ concentration range in a) DME and b) THF by DRS. The upper, blue curves represent measured real permittivity (ε') spectra while the lower, orange curves represent the measured imaginary permittivity (ε") spectra. Dashed lines represent extrapolated fits of these spectra incorporating one Debye and one Cole-Cole relaxation. c,d) Measured dipolar dispersion amplitudes ($\varepsilon_r - \varepsilon_\infty$) as a function of salt concentration in c) DME and d) THF. The values corresponding to the complex permittivity data displayed in a-b) fall along the steeply rising portion of the curve. The complex permittivity data measured at higher concentrations are shown in the supporting information, Figure S4.

The weak coordination strength of $BHFIP^-$ suggests that ion correlations would probably exist as long-lived SSIPs. Direct evidence for the existence and evolution of SSIP populations is afforded by DRS. Unlike most vibrational spectroscopic methods that are sensitive primarily to 1st-shell interactions, DRS can readily detect SSIPs due to their large dipole moment.[18] This sensitivity is demonstrated in Figure 2a-b, which compares the complex permittivity behavior as a function of $Ca(BHFIP)_2$ concentration in the 0.005-0.05 M range where the ion correlations are strongest. Both DME and THF based solutions exhibit two primary dipole relaxations: a high frequency solvent relaxation (f ~ 35 GHz and 63 GHz, respectively)

and a low frequency ion pair relaxation ($f \sim 0.5$ GHz). Numerical fitting of the ε' and ε" spectra allows extraction of the relevant dipole relaxation parameters (supporting information, Table S1 and S2). While the total solvent dipole amplitude decreases slightly across this concentration range, the amplitude of the apparent ion pair dipoles increases dramatically. This dipole population causes the total solution dielectric constants (ε_r) to exhibit a proportional increase with salt concentration, approximately doubling the neat solvent values at 0.05 M in both DME and THF (see supporting information, Figure S5). At higher concentrations (see supporting information Figure S4), the ion pair dipoles cease their proportionate increase in spectral contribution with concentration.

The changes in ε_r originating solely from dipole rotations are quantified from the fitted data by calculating each electrolyte's dipolar dispersion amplitude ($\varepsilon_r - \varepsilon_\infty$), which involves subtracting the high frequency intramolecular and electronic permittivity contributions. When ($\varepsilon_r - \varepsilon_\infty$) is plotted vs. salt concentration two distinct concentration regimes are observed (Figure 2c-d). From 0 to 0.05 M, the value of ($\varepsilon_r - \varepsilon_\infty$) increases sharply and almost linearly with concentration. At higher concentrations these values tend to decrease slightly before either increasing slightly (DME) or levelling off (THF). Changes in these values are related to the number of ion pair dipoles formed in solution (positive influence) as well as the irrotational binding of solvent to Ca^{2+} (negative influence). Irrotational binding typically includes solvent molecules beyond the 1st shell.[20] Based on an analysis of the fitted DRS data,[19-20] the number of irrotationally bound solvent molecules per Ca^{2+} (Z_{IB}) decreases from approximately 30 to 7-10 across the salt concentration range of 0.05-0.4 M (supporting information, Figure S5c). At 0.4 M the Z_{IB} values begin to approach the expected Ca^{2+} 1st shell coordination numbers of DME (4) and THF (6).[13] This reduced coupling of Ca^{2+} with solvent beyond its 1st shell at higher concentrations may further improve its mobility, providing a benefit beyond simple ion pair de-correlation. Nevertheless, the existence of two distinct concentration regimes in the dipolar dispersion amplitude (0.005-0.05 M and 0.05-0.4 M) is fully consistent with the two measured Λ regimes. This provides strong evidence that the rotationally correlated ions detected by DRS are the translationally correlated ions responsible for limiting Λ at low salt concentrations (0.01 M). Subsequent computational analysis (*vide infra*) confirms that these ion pairs are SSIPs.

Table 1. Calculated net dielectric increments (Δε) and relaxation frequencies (*f*) for various hypothesized electrolyte species from MD simulations.

	DME		***THF***	
Species[a]	Δε (M^{-1})	*f* (GHz)	Δε (M^{-1})	*f* (GHz)
Solvent	-	20 ± 1	-	52 ± 4
Ca^{2+}	-14 ± 1	-	-8.79 ± 0.04	-
$BHFIP^-$	-5.0 ± 0.1	-	-3.1 ± 0.4	-
$Ca(BHFIP)_2$	-2.7 ± 0.1	1.4 ± 0.2	-1.4 ± 0.1	1.2 ± 0.3
$Ca(BHFIP)^+_{CIP}$	48 ± 4	0.88 ± 0.20	44 ± 1	0.60 ± 0.16
$Ca(BHFIP)^+_{SSIP}$	363 ± 3	0.42 ± 0.08	257 ± 10	0.35 ± 0.05

[a]Explicit solvent molecules omitted for clarity

The local structures of the Ca-BHFIP ion pairs are identified by using MD simulations to determine the dielectric properties of various salt clusters and then comparing these with the measured DRS data. In the case of SSIPs, quantum chemistry was used to determine the geometry used in MD simulations (vide infra). The primary cluster property of interest from MD is the dielectric increment (Δε), which quantifies the impact that each species would have on the overall dipolar dispersion amplitude in solution. This method accounts for both the time-averaged dipole moment of the clusters themselves and their influence on overall solvent contributions. The calculated Δε values of the free ions, neutral clusters, and exemplar ion pair structures (CIP or SSIP) are shown in Table 1 along with each species' calculated relaxation frequency (*f*). The Δε values calculated for the free ions Ca^{2+} and $BHFIP^-$ are negative, demonstrating that complete dissociation of $Ca(BHFIP)_2$ into uncorrelated cations and anions would cause ε_r to decrease substantially with increasing salt concentration. This is because the ions themselves possess no net dipole moment and they reduce the total free solvent population through direct coordination and volumetric displacement, respectively. Similar arguments apply to the neutral $Ca(BHFIP)_2$ cluster, which also has a negative, albeit less so, Δε. By contrast, the computed Δε values for the $Ca(BHFIP)^+$ CIP clusters in DME and THF are quite large at 48 M^{-1} and 44 M^{-1}, respectively, owing to their large dipole moments. However, when these values are compared with the measured $(\varepsilon_r - \varepsilon_\infty)/c$ values of over 100 in the low concentration regime (see supporting information, Figure S5b), it becomes clear that these CIPs cannot explain the large measured

permittivity increase. Only SSIPs in which the anion exhibits a significant residence time in the second solvation shell of the cation (see Figure 3) can explain this increase. Due to the larger distance between the cation and anion in these clusters (i.e. larger dipole moment), the corresponding $\Delta\varepsilon$ values increase significantly to 363 (DME) and 257 M^{-1} (THF) , respectively. These large $\Delta\varepsilon$ values can thus account for the $(\varepsilon_r - \varepsilon_\infty)/c$ values measured in the low concentration regime. The differences in $\Delta\varepsilon$ values are primarily related to the preferred cation-anion distances, which are found to be larger in DME (Ca-B = 7.05 Å) than in THF (Ca-B = 5.83 Å) based on quantum chemical calculations. The predicted SSIP relaxation frequencies for these clusters (0.35-0.42 GHz) are somewhat lower than the measured frequencies (0.40-0.78 GHz), but this underestimation is consistent with the differences between the predicted and measured solvent frequencies as well. The combined quantum chemical calculations and MD simulations thus provide strong support for the assignment of SSIPs as the dominant ion pair species.

Representative solvation structures of the SSIP clusters and corresponding Ca-O radial distribution functions for solvent and anion are shown in Figure 3. These structures exhibit a well-defined 1st solvation shell of solvent oxygens followed by a less-defined 2nd shell of both solvent and anion oxygens. The 1st shell oxygen coordination number (*CN*) is approximately 8 in DME and 6 in THF, similar to previous X-ray based analyses of Ca^{2+} solvation in these solvents.[13] The 1st shell Ca-O_{solv} distances of 2.45 Å (DME) and 2.40 Å (THF) are also close to the reported experimental values.[13] Based on the previously mentioned Ca-B distances, THF allows closer approach of the $BHFIP^-$ in the 2nd shell, leading to smaller Ca-O_{BHFIP} distances. The larger number of DME oxygen atoms in the vicinity of Ca^{2+} as shown in the *CN* data is likely related to the larger fraction of oxygen atoms in DME compared to THF. This increased oxygen *CN* for DME is consistent with the Z_{IB} calculations from DRS fitting once the two oxygen atoms in DME are accounted for. For example, the Z_{IB} values calculated at 0.1 M are approximately 21 (DME) and 24 (THF), which correspond to Ca-O_{solv} *CN* values of 42 and 24, respectively. In the MD results shown in Figure 3, these values are reached at r = 9-10 Å in both solvents, demonstrating that the length-scale of irrotational solvent binding in these solutions extends beyond even the 2nd shell at these relatively low salt concentrations.

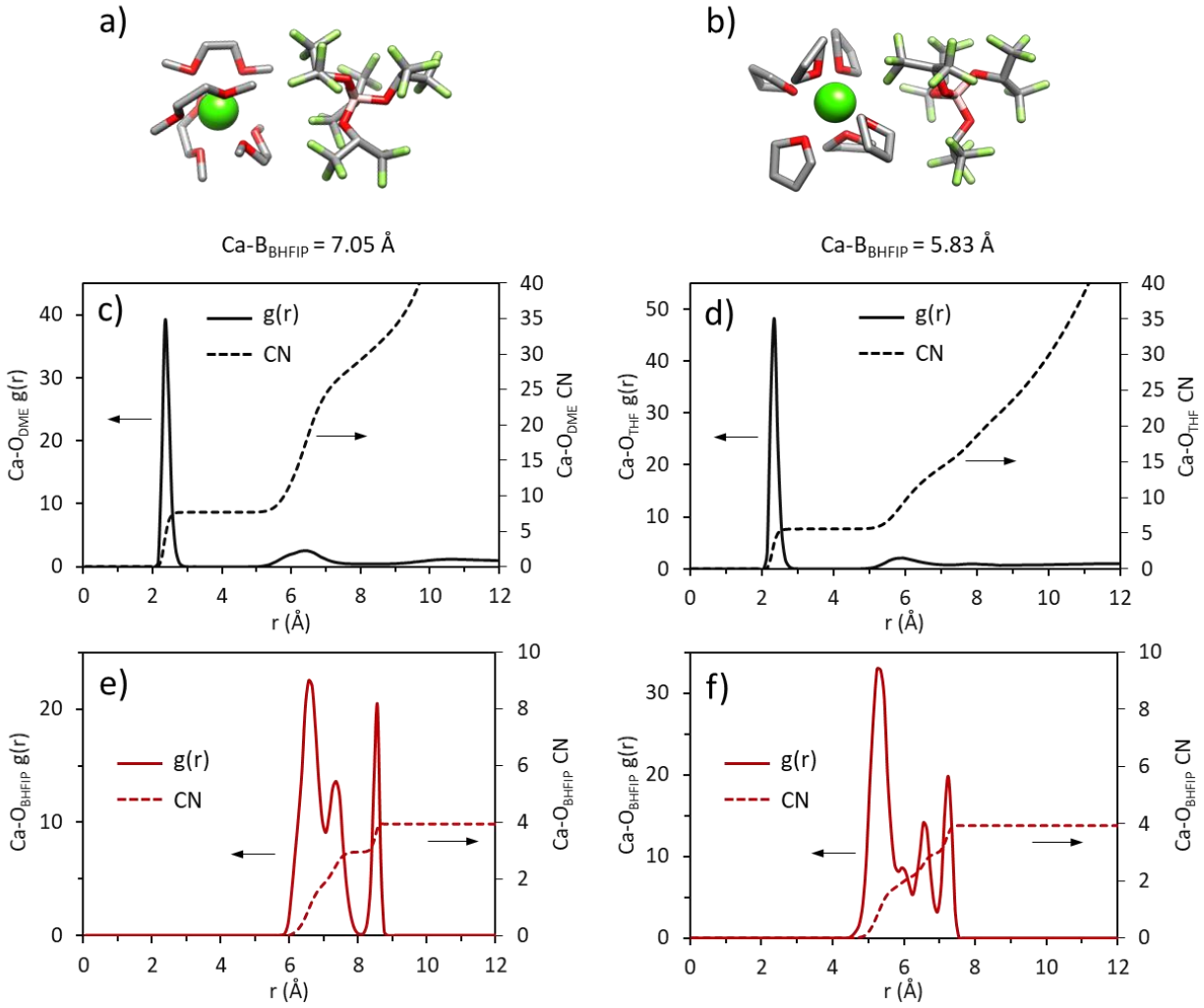

Figure 3. Local structure models and Ca-O radial distribution functions of the SSIP clusters derived from species-constrained MD simulations in a,c,e) DME and b,d,f) THF. Ca, O, F, C, and B atoms are depicted as green, red, green, gray, and pink, respectively; H atoms and non-1st shell solvent are omitted from the visual models. In these simulations, the Ca-B distance is first determined from quantum chemical calculations and is then fixed during the MD simulation to preserve existence of the SSIP.

Since the computed SSIP $\Delta\varepsilon$ values are greater than the measured $(\varepsilon_r - \varepsilon_\infty)/c$ values, the electrolytes likely contain an equilibrium mixture of SSIPs and free ions (eq. 2).

$$Ca^{2+} + 2BHFIP^- \leftrightarrow Ca(BHFIP)^+_{SSIP} + BHFIP^- \quad (2)$$

This equilibrium would be consistent with previously reported XAS data indicating CIP clusters are not prevalent.[12-13] Based on this equilibrium, the populations of SSIPs and free ions can be calculated from the computed $\Delta\varepsilon$ values and the measured $(\varepsilon_r - \varepsilon_\infty)/c$ values (Figure 4). This analysis reveals that the percentage

of the total Ca^{2+} inventory residing in SSIPs reaches a maximum of 60-70% at 0.01-0.02 M salt concentration and that this percentage decreases with increasing concentration, reaching 10-15% at 0.4 M. The similarity of these values whether the solvent is THF or DME demonstrates the generality of this speciation behavior in ether-based $Ca(BHFIP)_2$ electrolytes. Importantly, the concentration corresponding to minimum free Ca^{2+} derived from DRS agrees well with that of minimum Λ. The fact that the SSIP percentages are so significant at low salt concentrations despite the extreme charge delocalization of the $BHFIP^-$ anion is a testament to the strength of the long-range Coulombic interactions operating in ethereal multivalent electrolytes; the 1st solvent shell is incapable of eliminating these interactions and the anion therefore couples strongly to the cation in the 2nd solvation shell. Note that these SSIPs are likely highly dynamic but have residence times of at least 200-300 ps based on the DRS relaxation frequencies. From the perspective of electrochemical behavior, the important takeaway from Figure 4 is that the relative concentration of SSIPs in solution decreases significantly at elevated salt concentrations. Such entities likely behave differently from free Ca^{2+} at the electrified interface and may enhance anion degradation during cycling (*vide infra*).

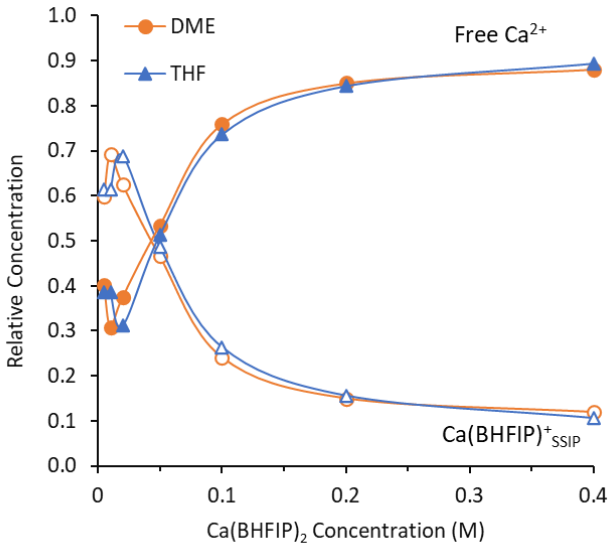

Figure 4. Relative Ca^{2+} species fractions as a function of overall salt concentration in DME and THF based on measured $(\varepsilon_r - \varepsilon_\infty)/c$ and calculated Δε values from Table 1 assuming an equilibrium between SSIPs (empty symbols) and free Ca^{2+} (filled symbols) according to eq. 1.

The driver for more effective de-correlation of SSIPs at higher salt concentrations likely originates from their large dipole moments, in accordance with a re-dissociation mechanism.[17, 45-46] Although the percentage of SSIPs in solution decreases, their absolute concentration generally increases with salt concentration. The increasing concentration of these strong dipoles, manifested as a significantly increased solution dielectric constant, serves to decrease the electrostatic interactions among the remaining free ions. In other words, the SSIPs may be thought of as a stochastic population of highly polar co-solvent molecules (albeit charged) that improves the de-correlated motion of the other ions.

The presence of the proposed distinct Ca^{2+} solvation environments at high and low salt concentrations was validated through X-ray Absorption Near Edge Spectroscopy (XANES) at the Ca K-edge. XANES is one of few experimental techniques, along with DRS, that enables characterization of extended solvation structures such as SSIPs. This is due to the significant influence of ligand symmetry on the unoccupied d and p orbitals of Ca^{2+} directly accessible to X-ray absorption techniques.[48-50] As such, it is uniquely poised to provide a complementary and element specific test for the presence of these species; whereas, other element specific spectroscopies, such as EXAFS, may only identify first shell solvent geometry since the SSIP EXAFS correlations are simply too far away to be effectively measured. The local Ca^{2+} solvation structure was thus probed within salt concentration regimes ostensibly containing either mostly free Ca^{2+} (0.4-0.45 M) or significant SSIPs (0.01 M). In comparing the XANES spectra measured at these two concentrations (Figure 5a,b), it is noteworthy that the two spectra maintain their basic pre-edge line-shape at approximately 4041 eV albeit with modest changes in intensity; in DME a single peak is observed while in THF two peaks are observed. Our previous work demonstrated that these solvent-dependent differences result from a difference in Ca-O coordination symmetry, with THF exhibiting octahedral, 6-fold O coordination to Ca^{2+} and DME exhibiting 7 or 8-fold coordination.[13] Therefore, it is clear that these basic differences in 1st shell coordination symmetry are maintained whether the $BHFIP^-$ anion is present in many of the second solvation shells (0.01 M) or not (0.4-0.45 M). However, the increase in pre-edge peak intensity for both DME and THF at the lower concentration, combined with a slight merging of the two peaks in THF, could indicate a slight distortion of these Ca-O interactions. A second

significant difference between the low and high concentration spectra is observed *via* the rising edge intensity at approximately 4045 eV. A large drop in the prominence of this feature is observed at 0.01 M. This suggests that Ca-solvent interactions beyond Ca-O coordination symmetry are impacted by the presence of $BHFIP^-$ in the second solvation shell.

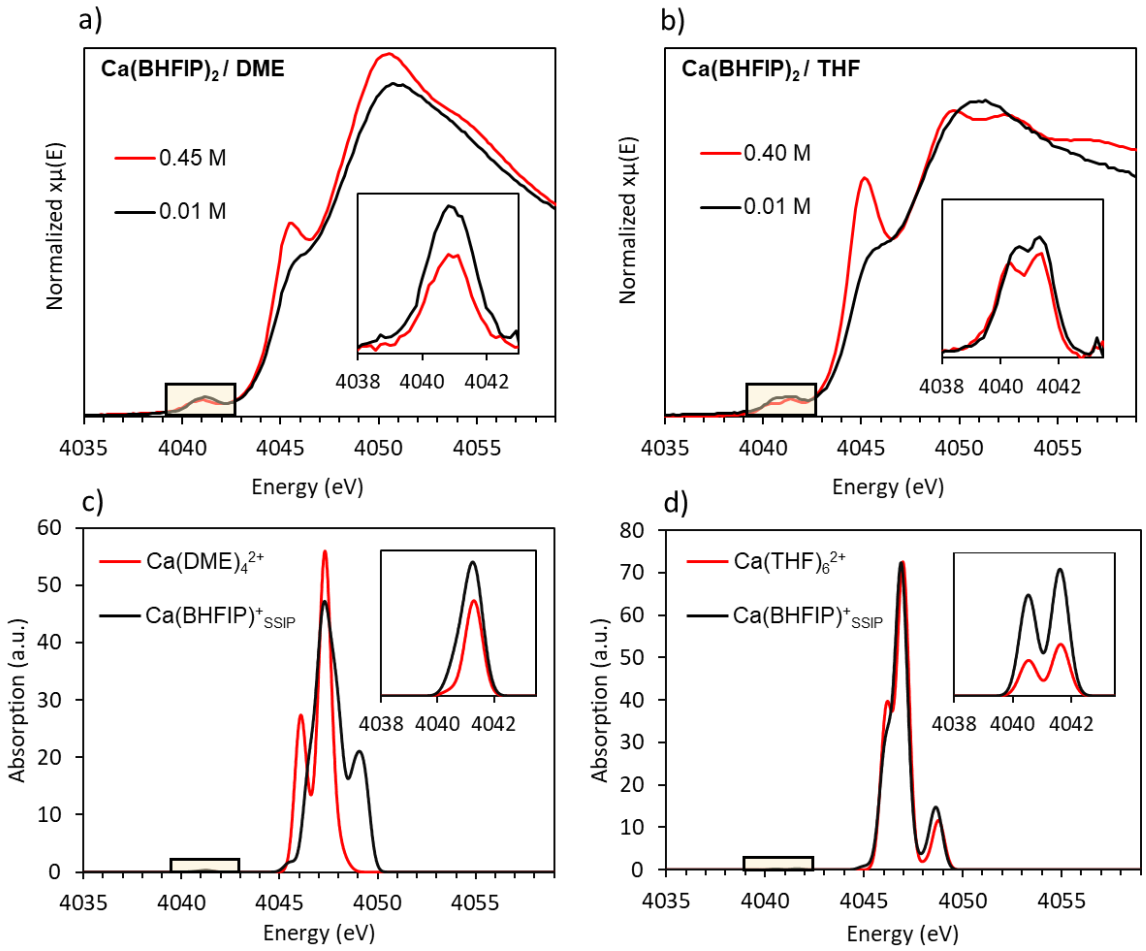

Figure 5. a,b) Measured Ca K-edge XANES at various salt concentrations in a) DME and b) THF. c,d) Simulated XANES absorption bands based on TD-DFT calculations of local Ca^{2+} solvation structures comparing the $Ca(BHFIP)^+$ SSIP and free Ca^{2+} cation in c) DME and d) THF. The insets show the background subtracted pre-edge region of the XANES. Theoretical spectra energy values were adjusted by +50.4 eV to match the experimental spectra

To validate the connection between these spectral differences and the local Ca^{2+} structure, time dependent Density Functional Theory (TD-DFT) was used to simulate XANES spectra for the structures of 8-fold coordinated $[Ca(DME)_4]^{2+}$ and 6-fold coordinated $[Ca(THF)_6]^{2+}$ both with and without the $BHFIP^-$

anion present in the second shell (Figure 5c,d). To reduce the computational cost, TD-DFT calculations were performed in presence of only one $BHFIP^-$ anion. Consistent with the concentration-dependent experimental measurements, when $BHFIP^-$ is present the pre-edge line shape is essentially maintained and the intensity is increased. This confirms that the basic Ca-O coordination symmetry is maintained in these two instances. Importantly, we also observed a reduction in the intensity of the rising-edge peak for the SSIP cluster. This is also consistent with the experimental spectral changes between the free Ca^{2+} (0.4-0.45 M) and the SSIP-enriched (0.01 M) regimes. The general agreement between the measured and simulated spectral changes supports the claim that the relative prevalence of the $Ca(BHFIP)^+_{SSIP}$ cluster is significantly enhanced at low salt concentrations in both DME and THF. In the THF case, the XANES spectrum of an additional SSIP structure involving a shorter Ca^{2+}-$BHFIP^-$ distance (i.e. tighter cation-anion binding) was simulated (supporting information, Figure S7a). The spectrum for this cluster exhibits even more significant changes in both pre-edge line-shape and rising-edge intensity confirming greater perturbation of the Ca^{2+} orbitals due to the proximity of $BHFIP^-$. The TD-DFT calculations were also performed for the THF SSIP cluster in the presence of an implicit THF solvent using the conductor-like polarizable continuum model (CPCM).[51] Inclusion of the implicit solvent did not change these results (supporting information, Figure S7b). The combined XANES and TD-DFT results provide clear experimental evidence of perturbation to the electronic orbitals of Ca^{2+} as a result of significant SSIP populations.

Elucidation of the electronic transitions giving rise to the spectral features of the XANES region reveals that the 2nd shell $BHFIP^-$ anion impacts 1st shell solvent structure. The natural transition orbitals[52] and corresponding atomic orbital contributions for the spectra are shown in Figure S7. In this region, the relevant electronic excitations are those occurring from the Ca 1s orbitals to higher energy orbitals. The lower energy rising edge peak (states 16 and 20) shows contributions from the Ca 4p orbitals mixed with Ca 4s along with C and H contributions from the THF ligands (supporting information, Table S4). The higher energy rising edge peak (states 24 and 26) has contributions from Ca 3d and 4p mixed with THF-ligand contributions. Particularly for state 26, we observed the contribution coming from both O and C of the THF-ligand mixed with the Ca 4p and 3d, making the excited state more delocalized. This explains the

high intensity absorption in this region. Interestingly, we observed that the Ca 3p orbitals are deep inside the occupied energy range and that they were not involved in any of the Ca 1s excitations. Given that the excited states within the rising-edge region are composed of a mixture of orbitals from Ca and the coordinating solvent atoms (especially C and H), the reduction in rising-edge intensity resulting from SSIP formation indicates that the presence of $BHFIP^-$ within the second solvation shell slightly modifies or distorts the average orientation of the 1st shell solvent molecules with respect to Ca^{2+}. However, this modification appears primarily restricted to the hydrocarbon backbone of the solvent molecules, leaving the Ca-O geometry largely unperturbed unless the cation-anion distance becomes shorter (c.f. Figure S7a).

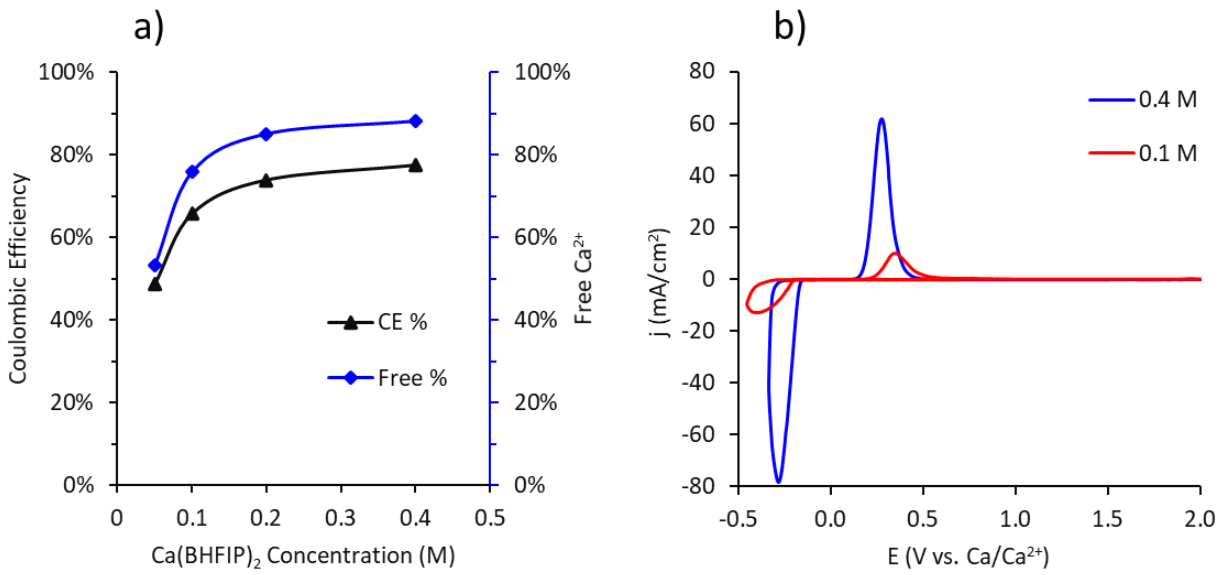

Figure 6. a) Calcium cycling Coulombic efficiencies (CE) measured by cyclic voltammetry (CV) on gold substrates at various $Ca(BHFIP)_2$ concentrations in DME. CV scan rates of 50 mV/s were used and real-time *IR* correction was applied. Various cathodic endpoints between -0.32 to -0.5 V were tested and the CE values are reported for the best conditions in each case. The relative free Ca^{2+} percentage is reproduced from Figure 4 for comparison. b) Example CV curves measured at 0.4 M and 0.1 M $Ca(BHFIP)_2$ in DME demonstrating the effects of concentration on the measured CV response. Additional CV curves are shown in the supporting information, Figure S8.

The relative prevalence of free (non SSIP) Ca^{2+} in solution, as controlled by the salt concentration, correlates strongly with electrochemical calcium metal cycling efficiency. The ratio of anodic to cathodic charge passed during calcium stripping and plating, respectively, i.e. Coulombic efficiency (CE), is a measure of electrolyte reductive stability during the calcium cycling process. Comparisons of the CE values

measured during early-stage CV cycling of calcium on gold substrates reveals a positive dependence on salt concentration across the relevant concentration of 0.05-0.4 M in DME (Figure 6a). Difficulties in producing a THF solvate salt of sufficient purity for high CE calcium cycling prevented a parallel electrochemical investigation in THF. Electrolytes at the highest concentrations yielded CE values > 70 %, generally consistent with literature values,[9, 11, 53] although no standard set of conditions for calcium cycling have been established. In this work, we apply real-time correction for the measured uncompensated resistance between the working and reference electrodes at each concentration. This ensures better accuracy of the measured potential and thus more consistent potential scanning conditions.[54] We find that even at a concentration of 0.4 M, where ionic conductivity is high (10 mS/cm), significant uncompensated resistance effects are present in the 3-electrode beaker cell format (see supporting information, Figure S9). After accounting for these effects, we find that reducing the salt concentration leads to a reduction in both current density (Figure 6b) and CE value. The former indicates reduced charge-transfer kinetics along with a modest increase in concentration overpotential while the latter indicates increased parasitic loss due to electrolyte reduction. The charge-transfer kinetics and parasitic loss are probably linked, but a thorough investigation of this relationship is beyond the scope of this work.

As shown in Figure 6a we find a strong correlation between the relative free Ca^{2+} population and the calcium cycling performance of the electrolyte. Given the established reductive susceptibility of the $BHFIP^-$ anion during calcium cycling leading to fluoride-based film formation,[11, 53, 55] we propose the anion as the primary source of the instability during calcium cycling in these electrolytes. In consideration of the speciation changes occurring as a function of concentration, it appears that the presence of $BHFIP^-$ in the 2^{nd}-shell of Ca^{2+} leads to an increased likelihood of decomposition. This link may be intuitively rationalized by the SSIPs favoring Ca^{2+}-mediated transport of $BHFIP^-$ anions to the electrode surface during calcium plating. Furthermore, electrostatic interactions between $BHFIP^-$ and the polarizing Ca^{2+} cation may alter the anion's reductive susceptibility, based on previous investigations of salt stability in similar multivalent electrolytes.[10, 55-56] Our XAS results further reveal that the 2^{nd}-shell anion slightly distorts the 1^{st} solvation shell, which may exacerbate these issues. These findings demonstrate that ion interactions beyond the 1^{st}

solvation shell are important not just for conductivity, but for electrolyte stability as well. Therefore, we propose the unexpected design consideration that reducing salt concentration may increase the likelihood of anion decomposition in ether-based multivalent electrolytes.

Conclusions

To better understand the links between multivalent cation solvation environments and ensemble electrolyte behavior, we have investigated the concentration-dependent behavior of the state-of-the-art calcium salt $Ca(BHFIP)_2$ in exemplar ether solvents. We find that the effective ionicity of these electrolytes follows a non-monotonic trend indicative of non-intuitive ion correlations that are largely independent of the specific ether solvent structure. These correlations result in the observation of a Λ minimum at concentrations near 0.01 M followed by a large increase in Λ with increasing concentration. Based on the measured complex permittivity behavior over this concentration range, we identify these correlations as discrete $Ca(BHFIP)^+_{SSIP}$ ion pairs with correlated lifetimes of several hundred ps or more. Complementary solvation structure analysis through XAS-TD-DFT supports the proposed changes in free vs. SSIP Ca^{2+} across these concentration regimes. The large dipole moments of the SSIP species likely assist in the mitigation of Coulombic interactions at elevated concentrations, resulting in greater populations of free Ca^{2+}. The calcium cycling behavior of these electrolytes reveals a significant correlation between electrolyte stability and the fraction of free Ca^{2+} in the system. These findings demonstrate that even the weakest associating multivalent salts exhibit significant correlations via ion pairing in ether solvents. The counter-intuitive concentration dependence of these correlations exhibits a measurable impact on electrochemical properties.

Author Contributions

NTH synthesized the electrolytes, performed the electrochemical and dielectric relaxation spectroscopy measurements, coordinated the contributing investigations, and wrote the original draft; JS and KAP performed the molecular dynamics simulations and electronic structure calculations; DMD and MB performed the X-ray absorption spectroscopy measurements; ND and LAC performed the time-dependent

density functional theory simulations; KSH, VM and KTM performed the pulsed-field gradient nuclear magnetic resonance measurements and analysis; KRZ assisted in the design and interpretation of the electrochemical measurements. All authors contributed to the review and editing of the manuscript.

Conflicts of Interest

There are no conflicts of interest to declare.

Acknowledgements

This work was led and supported by the Joint Center for Energy Storage Research, an Energy Innovation Hub funded by the U.S. Department of Energy. Sandia National Laboratories is a multimission laboratory managed and operated by National Technology & Engineering Solutions of Sandia, LLC, a wholly owned subsidiary of Honeywell International Inc., for the U.S. Department of Energy's National Nuclear Security Administration under contract DE-NA0003525. This research used resources of the National Energy Research Scientific Computing Center, a DOE Office of Science User Facility supported by the Office of Science of the U.S. Department of Energy under contract no. DE-AC02-05CH11231. This research used resources of the Advanced Photon Source, an Office of Science User Facility operated for the U.S. Department of Energy (DOE) Office of Science by Argonne National Laboratory and was supported by the U.S. DOE under Contract No. DE-AC02-06CH11357. We gratefully acknowledge George E. Sterbinsky for his valuable assistance in the operation of beamline 9-BM. We acknowledge Laboratory Computing Resource Center (LCRC, Bebop) for the use of simulation resources. We thank Prof. Samuel Odoh, University of Nevada, Reno, for assistance with extracting orbital contributions information from ORCA. The PFG-NMR measurements were performed at the Environmental Molecular Sciences Laboratory (EMSL), a national scientific user facility sponsored by the DOE's Office of Biological and Environmental Research and located at Pacific Northwest National Laboratory (PNNL). This paper describes objective technical results and analysis. Any subjective views or opinions that might be expressed in the paper do not necessarily represent the views of the U.S. Department of Energy or the United States Government.

Supporting Information. The following files are available free of charge. Dielectric increment calculations, conductivity measurements, PFG-NMR self-diffusion coefficients, DRS spectra and derived parameters, ion pair structures from MD, calculated XAS-TD-DFT spectrum and excited state orbital diagrams/assignments, CV plots.

References

1. Hahn, N. T.; Self, J.; Seguin, T. J.; Driscoll, D. M.; Rodriguez, M. A.; Balasubramanian, M.; Persson, K. A.; Zavadil, K. R., The critical role of configurational flexibility in facilitating reversible reactive metal deposition from borohydride solutions. *Journal of Materials Chemistry A* **2020**.
2. Arroyo-de Dompablo, M. E.; Ponrouch, A.; Johansson, P.; Palacín, M. R., Achievements, Challenges, and Prospects of Calcium Batteries. *Chemical Reviews* **2019**.
3. Canepa, P.; Gautam, G. S.; Hannah, D. C.; Malik, R.; Liu, M.; Gallagher, K. G.; Persson, K. A.; Ceder, G., Odyssey of Multivalent Cathode Materials: Open Questions and

Future Challenges. *Chem. Rev.* **2017,** *117*, 4287-4341.
4. Mizrahi, O.; Amir, N.; Pollak, E.; Chusid, O.; Marks, V.; Gottlieb, H.; Larush, L.; Zinigrad, E.; Aurbach, D., Electrolyte Solutions with a Wide Electrochemical Window for Rechargeable Magnesium Batteries. *Journal of The Electrochemical Society* **2008,** *155* (2), A103-A109.
5. Viestfrid, Y.; Levi, M. D.; Gofer, Y.; Aurbach, D., Microelectrode studies of reversible Mg deposition in THF solutions containing complexes of alkylaluminum chlorides and dialkylmagnesium. *Journal of Electroanalytical Chemistry* **2005,** *576* (2), 183-195.
6. Wang, D.; Gao, X.; Chen, Y.; Jin, L.; Kuss, C.; Bruce, P. G., Plating and stripping calcium in an organic electrolyte. *Nature Materials* **2017,** *17*, 16.
7. Herb, J. T.; Nist-Lund, C. A.; Arnold, C. B., A Fluorinated Alkoxyaluminate Electrolyte for Magnesium-Ion Batteries. *ACS Energy Letters* **2016,** *1* (6), 1227-1232.
8. Zhao-Karger, Z.; Bardaji, M. E. G.; Fuhr, O.; Fichtner, M., A new class of non-corrosive, highly efficient electrolytes for rechargeable magnesium batteries. *Journal of Materials Chemistry A* **2017,** *5* (22), 10815-10820.
9. Li, Z.; Fuhr, O.; Fichtner, M.; Zhao-Karger, Z., Towards stable and efficient electrolytes for room-temperature rechargeable calcium batteries. *Energy & Enviromental Science* **2019,** *10.1039/c9ee01699f*.
10. Lau, K.-C.; Seguin, T. J.; Carino, E. V.; Hahn, N. T.; Connell, J. G.; Ingram, B. J.; Persson, K. A.; Zavadil, K. R.; Liao, C., Widening Electrochemical Window of Mg Salt by Weakly Coordinating Perfluoroalkoxyaluminate Anion for Mg Battery Electrolyte. *Journal of The Electrochemical Society* **2019,** *166* (8), A1510-A1519.
11. Shyamsunder, A.; Blanc, L. E.; Assoud, A.; Nazar, L. F., Reversible Calcium Plating and Stripping at Room Temperature Using a Borate Salt. *ACS Energy Letters* **2019,** *4* (9), 6.
12. Hahn, N. T.; Driscoll, D. M.; Yu, Z.; Sterbinsky, G. E.; Cheng, L.; Balasubramanian, M.; Zavadil, K. R., Influence of Ether Solvent and Anion Coordination on Electrochemical Behavior in Calcium Battery Electrolytes. *ACS Applied Energy Materials* **2020,** *3* (9), 8437-8447.

13. Driscoll, D. M.; Dandu, N. K.; Hahn, N. T.; Seguin, T. J.; Persson, K. A.; Zavadil, K. R.; Curtiss, L. A.; Balasubramanian, M., Rationalizing Calcium Electrodeposition Behavior by Quantifying Ethereal Solvation Effects on Ca2+ Coordination in Well-Dissociated Electrolytes. *Journal of The Electrochemical Society* **2020,** *167* (16), 160512.
14. Forero-Saboya, J. D.; Marchante, E.; Araujo, R. B.; Monti, D.; Johansson, P.; Ponrouch, A., Cation Solvation and Physicochemical Properties of Ca Battery Electrolytes. *The Journal of Physical Chemistry C* **2019,** *123* (49), 29524-29532.
15. Samuel, D.; Steinhauser, C.; Smith, J. G.; Kaufman, A.; Radin, M. D.; Naruse, J.; Hiramatsu, H.; Siegel, D. J., Ion Pairing and Diffusion in Magnesium Electrolytes Based on Magnesium Borohydride. *ACS Applied Materials & Interfaces* **2017,** *9* (50), 43755-43766.
16. Hahn, N. T.; Self, J.; Han, K. S.; Murugesan, V.; Mueller, K. T.; Persson, K. A.; Zavadil, K. R., Quantifying Species Populations in Multivalent Borohydride Electrolytes. *The Journal of Physical Chemistry B* **2021,** *125* (14), 3644-3652.
17. Self, J.; Hahn, N. T.; Fong, K. D.; McClary, S. A.; Zavadil, K. R.; Persson, K. A., Ion pairing and redissociaton in low-permittivity electrolytes for multivalent battery applications. *The Journal of Physical Chemistry Letters* **2020,** *11* (6), 2046-2052.
18. Buchner, R.; Hefter, G., Interactions and dynamics in electrolyte solutions by dielectric spectroscopy. *Physical Chemistry Chemical Physics* **2009,** *11* (40), 8984-8999.
19. Buchner, R.; Hefter, G. T.; May, P. M., Dielectric Relaxation of Aqueous NaCl Solutions. *The Journal of Physical Chemistry A* **1999,** *103* (1), 1-9.
20. Buchner, R.; Chen, T.; Hefter, G., Complexity in "simple" electrolyte solutions: Ion pairing in MgSO4(aq). *The Journal of Physical Chemistry B* **2004,** *108* (7), 2365-2375.
21. Ravel, B.; Newville, M., ATHENA, ARTEMIS, HEPHAESTUS: data analysis for X-ray absorption spectroscopy using IFEFFIT. *Journal of Synchrotron Radiation* **2005,** *12* (4), 537-541.
22. Newville, M., Larch: An Analysis Package for XAFS and Related Spectroscopies. *Journal of Physics: Conference Series* **2013,** *430*, 012007.
23. Self, J.; Wood, B. M.; Rajput, N. N.; Persson, K. A., The Interplay between Salt Association and the Dielectric Properties of Low Permittivity Electrolytes: The Case of LiPF6 and LiAsF6 in Dimethyl Carbonate. *The Journal of Physical Chemistry C* **2018,** *122* (4), 1990-1994.
24. Martínez, L.; Andrade, R.; Birgin, E. G.; Martínez, J. M., PACKMOL: A Package for Building Initial Configurations for Molecular Dynamics Simulations. *J. Comput. Chem.* **2009,** *30*, 2157-2164.
25. Abraham, M. J.; Murtola, T.; Schulz, R.; Páll, S.; Smith, J. C.; Hess, B.; Lindahl, E., GROMACS: High Performance Molecular Simulations through Multi-Level Parallelism from Laptops to Supercomputers. *SoftwareX* **2015,** *1-2*, 19-25.
26. Berendsen, H. J. C.; Postma, J. P. M.; Gunsteren, W. F. v.; DiNola, A.; Haak, J. R., Molecular dynamics with coupling to an external bath. *The Journal of Chemical Physics* **1984,** *81* (8), 3684-3690.
27. Bussi, G.; Donadio, D.; Parrinello, M., Canonical sampling through velocity rescaling. *The Journal of Chemical Physics* **2007,** *126* (1), 014101.
28. Caleman, C.; van Maaren, P. J.; Hong, M.; Hub, J. S.; Costa, L. T.; van der Spoel, D., Force Field Benchmark of Organic Liquids: Density, Enthalpy of Vaporization, Heat Capacities, Surface Tension, Isothermal Compressibility, Volumetric Expansion Coefficient, and Dielectric Constant. *J. Chem. Theory Comput.* **2012,** *8*, 61-74.

29. Jorgensen, W. L.; Maxwell, D. S.; Tirado-Rives, J., Development and Testing of the OPLS All-Atom Force Field on Conformational Energetics and Properties of Organic Liquids. *Journal of the American Chemical Society* **1996,** *118* (45), 11225-11236.
30. Kaminski, G. A.; Friesner, R. A.; Tirado-Rives, J.; Jorgensen, W. L., Evaluation and Reparametrization of the OPLS-AA Force Field for Proteins via Comparison with Accurate Quantum Chemical Calculations on Peptides. *The Journal of Physical Chemistry B* **2001,** *105* (28), 6474-6487.
31. *MacroModel*, Schrodinger, LLC: New York, NY, 2018.
32. Frisch, M. J.; Trucks, G. W.; Schlegel, H. B.; Scuseria, G. E.; Robb, M. A.; Cheeseman, J. R.; Scalmani, G.; Barone, V.; Petersson, G. A.; Nakatsuji, H., Gaussian 16 Rev. B.01 Release Notes. Wallingford, CT, 2016.
33. Chai, J.-D.; Head-Gordon, M., Long-range corrected hybrid density functionals with damped atom–atom dispersion corrections. *Physical Chemistry Chemical Physics* **2008,** *10* (44), 6615-6620.
34. Cancès, E.; Mennucci, B.; Tomasi, J., A new integral equation formalism for the polarizable continuum model: Theoretical background and applications to isotropic and anisotropic dielectrics. *The Journal of Chemical Physics* **1997,** *107* (8), 3032-3041.
35. Mennucci, B., Polarizable continuum model. *WIREs Computational Molecular Science* **2012,** *2* (3), 386-404.
36. Staroverov, V. N.; Scuseria, G. E.; Tao, J.; Perdew, J. P., Comparative assessment of a new nonempirical density functional: Molecules and hydrogen-bonded complexes. *The Journal of Chemical Physics* **2003,** *119* (23), 12129-12137.
37. Neese, F., The ORCA program system. *WIREs Computational Molecular Science* **2012,** *2* (1), 73-78.
38. Becke, A. D., A new mixing of Hartree–Fock and local density-functional theories. *The Journal of Chemical Physics* **1993,** *98* (2), 1372-1377.
39. Weigend, F.; Ahlrichs, R., Balanced basis sets of split valence, triple zeta valence and quadruple zeta valence quality for H to Rn: Design and assessment of accuracy. *Physical Chemistry Chemical Physics* **2005,** *7* (18), 3297-3305.
40. Saar, D.; Brauner, J.; Farber, H.; Petrucci, S., Dielectric relaxation of some 1:1 electrolytes in tetrahydrofuran and diethyl carbonate. *The Journal of Physical Chemistry* **1978,** *82* (17), 1943-1947.
41. Farber, H.; Petrucci, S., Electrical conductance, ultrasonic relaxation, and microwave dielectric relaxation of sodium perchlorate in tetrahydrofuran. *The Journal of Physical Chemistry* **1976,** *80* (3), 327-335.
42. Ashby, E. C.; Dobbs, F. R.; Hopkins, H. P., Composition of complex aluminum hydrides and borohydrides, as inferred from conductance, molecular association, and spectroscopic studies. *Journal of the American Chemical Society* **1973,** *95* (9), 2823-2829.
43. Lee, A. A.; Perez-Martinez, C. S.; Smith, A. M.; Perkin, S., Scaling Analysis of the Screening Length in Concentrated Electrolytes. *Physical Review Letters* **2017,** *119* (2), 026002.
44. Fuoss, R. M.; Kraus, C. A., Properties of Electrolytic Solutions. IV. The Conductance Minimum and the Formation of Triple Ions Due to the Action of Coulomb Forces. *Journal of the American Chemical Society* **1933,** *55* (6), 2387-2399.
45. Petrucci, S.; Masiker, M. C.; Eyring, E. M., The Possible Presence of Triple Ions in Electrolyte Solutions of Low Dielectric Permittivity. *Journal of Solution Chemistry* **2008,** *37* (7), 1031-1035.

46. Cavell, E. A. S.; Knight, P. C., Effect of concentration changes on permittivity of electrolyte solutions. *Zeitschrift für Physikalische Chemie* **1968,** *57* (3_6), 331.
47. Petrowsky, M.; Frech, R.; Suarez, S. N.; Jayakody, J. R. P.; Greenbaum, S., Investigation of fundamental transport properties and thermodynamics in diglyme−salt solutions. *The Journal of Physical Chemistry B* **2006,** *110* (46), 23012-23021.
48. Aziz, E. F.; Eisebitt, S.; de Groot, F.; Chiou, J. W.; Dong, C.; Guo, J.; Eberhardt, W., Direct Contact versus Solvent-Shared Ion Pairs in NiCl2 Electrolytes Monitored by Multiplet Effects at Ni(II) L Edge X-ray Absorption. *The Journal of Physical Chemistry B* **2007,** *111* (17), 4440-4445.
49. Fulton, J. L.; Heald, S. M.; Badyal, Y. S.; Simonson, J. M., Understanding the Effects of Concentration on the Solvation Structure of Ca2+ in Aqueous Solution. I: The Perspective on Local Structure from EXAFS and XANES. *The Journal of Physical Chemistry A* **2003,** *107* (23), 4688-4696.
50. Wildman, A.; Martinez-Baez, E.; Fulton, J.; Schenter, G.; Pearce, C.; Clark, A. E.; Li, X., Anticorrelated Contributions to Pre-edge Features of Aluminate Near-Edge X-ray Absorption Spectroscopy in Concentrated Electrolytes. *The Journal of Physical Chemistry Letters* **2018,** *9* (10), 2444-2449.
51. Barone, V.; Cossi, M., Quantum Calculation of Molecular Energies and Energy Gradients in Solution by a Conductor Solvent Model. *The Journal of Physical Chemistry A* **1998,** *102* (11), 1995-2001.
52. Martin, R. L., Natural transition orbitals. *The Journal of Chemical Physics* **2003,** *118* (11), 4775-4777.
53. Nielson, K. V.; Luo, J.; Liu, T. L., Optimizing Calcium Electrolytes by Solvent Manipulation for Calcium Batteries. *Batteries & Supercaps* **2020,** *3* (8), 766-772.
54. Connell, J. G.; Genorio, B.; Lopes, P. P.; Strmcnik, D.; Stamenkovic, V. R.; Markovic, N. M., Tuning the Reversibility of Mg Anodes via Controlled Surface Passivation by H2O/Cl- in Organic Electrolytes. *Chem. Mater.* **2016,** *28*, 8268-8277.
55. Yamijala, S. S. R. K. C.; Kwon, H.; Guo, J.; Wong, B. M., Stability of Calcium Ion Battery Electrolytes: Predictions from Ab Initio Molecular Dynamics Simulations. *ACS Applied Materials & Interfaces* **2021,** *13* (11), 13114-13122.
56. Rajput, N. N.; Qu, X.; Sa, N.; Burrell, A. K.; Persson, K. A., The Coupling between Stability and Ion Pair Formation in Magnesium Electrolytes from First-Principles Quantum Mechanics and Classical Molecular Dynamics. *Journal of the American Chemical Society* **2015,** *137* (9), 3411-3420.